HHS Public Access

Author manuscript

Neuroscience. Author manuscript; available in PMC 2024 April 15.

Published in final edited form as:

Neuroscience. 2023 April 15; 516: 113–124. doi:10.1016/j.neuroscience.2023.01.009.

Progressive spread of beta-amyloid pathology in an olfactory-driven APP mouse model

Helen C. Murray[1,2,*], **Galit Saar**[2,5], **Li Bai**[3], **Nadia Bouraoud**[2], **Stephen Dodd**[2], **Blake Highet**[1,6], **Brigid Ryan**[1], **Maurice A. Curtis**[1], **Alan Koretsky**[2,*], **Leonardo Belluscio**[4]

[1]Department of Anatomy and Medical Imaging and Centre for Brain Research, Faculty of Medical and Health Science, University of Auckland, Auckland, 1023, New Zealand.

[2]Laboratory of Functional and Molecular Imaging, National Institute of Neurological Disorders and Stroke, National Institutes of Health, Bethesda, MD 20892, USA.

[3]Circuits, Synapses and Molecular Signaling Section, National Institute of Neurological Disorders and Stroke, National Institutes of Health, Bethesda, MD 20892, USA

[4]Howard Hughes Medical Institute, Chevy Chase, MD 20815, USA

[5]The current affiliation of Galit Saar is Biomedical Core Facility, Faculty of Medicine, Technion-Israel Institute of Technology, Haifa, 3200003, Israel.

[6]The current affiliation of Blake Highet is Department of Neurobiology, University of Utah, Salt Lake City, UT 84112, USA

Abstract

Years before Alzheimer's disease (AD) is diagnosed, patients experience an impaired sense of smell, and β-amyloid plaques accumulate within the olfactory mucosa and olfactory bulb (OB). The olfactory vector hypothesis proposes that external agents cause β-amyloid to aggregate and spread from the OB to connected downstream brain regions. To reproduce the slow accumulation of β-amyloid that occurs in human AD, we investigated the progressive accumulation of β-amyloid across the brain using a conditional mouse model that overexpresses a humanized mutant form of the amyloid precursor protein (hAPP) in olfactory sensory neurons. Using design-based stereology, we show the progressive accumulation of β-amyloid plaques within the OB and cortical olfactory regions with age. We also observe reduced OB volumes in these mice when hAPP expression begins prior-to but not post-weaning which we tracked using manganese-

[*]**Corresponding authors:** Dr Alan Koretsky: KoretskyA@ninds.nih.gov; Dr Helen Murray: h.murray@auckland.ac.nz.

Author Contributions

H.C.M., A.K. and L. Belluscio. contributed to the conception and design of the experiments. Tissue processing was performed by H.C.M., L. Bai and N.B. Immunohistochemistry was performed by H.C.M. and L. Bai. Validation of hAPP mRNA expression was performed by B.R. and B.H. Magnetic resonance imaging was performed by G.S. and S.D. Data collection and interpretation were carried out by H.M. with critical revision by A.K. and M.A.C. The manuscript was prepared by H.M. with critical revision by M.A.C., L. Belluscio and A.K. and feedback from all authors. All authors have approved the final manuscript.

Competing Interests Statement

The authors declare no competing interests.

enhanced MRI. We therefore conclude that the reduced OB volume does not represent progressive degeneration but rather disrupted OB development. Overall, our data demonstrate that hAPP expression in the olfactory epithelium can lead to the accumulation and spread of β-amyloid through the olfactory system into the hippocampus, consistent with an olfactory system role in the early stages of β-amyloid-related AD progression.

Keywords

olfactory bulb; olfactory sensory neurons; anterior olfactory nucleus; Alzheimer's disease; Amyloid precursor protein; β-amyloid

Introduction:

Olfactory dysfunction is a common symptom in the earliest stages of Alzheimer's disease (AD), often occurring many years before the diagnostic memory and cognitive symptoms (Devanand et al., 2000; Attems et al., 2005). During the prodromal phase of the disease, the hallmark aggregates of β-amyloid and hyper-phosphorylated tau progressively accumulate in interconnected brain regions in a conserved pattern classified by Thal and Braak staging, respectively (Braak and Braak, 1995; Thal et al., 2002). β-amyloid and tau accumulate in the olfactory bulb (OB) of AD cases with low Braak staging, indicating that the olfactory system is one of the first regions affected by aggregate pathology (Kovács et al., 2001; Murray et al., 2020). A prominent theory of AD pathogenesis is the 'olfactory vector hypothesis' in which xenobiotics, metals or pollution lead to β-amyloid accumulation and seeding in olfactory sensory neurons (OSNs) within the olfactory epithelium (OE) of the nose (Doty, 2008; Dando et al., 2014; Rey et al., 2018). OSNs project directly through the cribriform plate into the OB which connects to olfactory regions and other downstream brain regions (Doty, 2008; Walker, 2018). Thus, the OB has a unique proximity to the external environment but is also a conduit to key forebrain structures.

β-amyloid and tau aggregates are detected in the OE of AD patients and the severity of this pathology correlates with the amount of cortical β-amyloid in the rest of the brain (Arnold et al., 2010). Furthermore, *in-vitro* studies have demonstrated that β-amyloid can be taken up by neurons, transferred to other cells in an anterograde or retrograde direction and can seed aggregation in the new cell (Koo et al., 1990; Morales et al., 2015; Olsson et al., 2018). A recent in-vivo study also demonstrated that β-amyloid injected into the OB spreads to connected brain regions and causes apoptosis over an acute 3-day period (He et al., 2018).

However, in the AD brain the accumulation of β-amyloid in the OE and OB is likely to be a slow process during aging. To simulate a more chronic process, we used a conditional model of olfactory-driven amyloid pathology. This mouse model expresses humanized amyloid precursor protein (hAPP) carrying the "Swedish" and "Indiana" familial APP mutations in mature OSNs. Overexpression of the hAPP gene is controlled by tetracycline transactivator (tTA) which is driven by the olfactory marker protein (OMP) promoter as previously described (Cheng et al., 2011). We refer to this line as OMP-hAPP mice. Using this tet-off system, spatial and temporal control of the transgene expression is achieved using Doxycycline (Dox, Figure 1a, b). Furthermore, by crossing OMP-hAPP mice with

a null β-site APP cleaving enzyme 1 ($BACE^{-/-}$) line, an OMP-hAPP-$BACE^{-/-}$ line was generated which does not form β-amyloid plaques (Cheng et al., 2016). The OMP-hAPP and OMP-hAPP-$BACE^{-/-}$ mice both show OSN apoptosis and olfactory dysfunction by 3 weeks of age, demonstrating that the OSN loss occurred independently of β-amyloid formation (Cheng et al., 2011, 2013, 2016). Therefore, the purpose of the present study was to assess whether β-amyloid produced in the OE progressively accumulates in the OB and downstream brain regions, and whether any atrophy in these regions is dependent upon β-amyloid plaque production.

We used a design-based stereology approach to assess plaque accumulation in the OB, anterior olfactory nucleus (AON), piriform cortex (PIR) and hippocampus (HP) of OMP-hAPP mice at 6-, 12-, 18- and 24-months of age. We also assessed the volume of these regions in OMP-hAPP and OMP-hAPP-$BACE^{(-/-)}$ mice to determine whether plaque accumulation is associated with neurodegeneration. Lastly, manganese-enhanced MRI (MEMRI) was used to track the change in OB volume with age.

Our results demonstrate that expression of $hAPP_{swe,ind}$ in the OSNs results in the progressive accumulation of β-amyloid plaques throughout the olfactory system and downstream cortical regions with age. This finding implicates the olfactory system in the earliest stages of β-amyloid accumulation in Alzheimer's disease.

Results

Beta-amyloid deposition progresses along the olfactory pathway

Extracellular β-amyloid deposits were observed in OMP-hAPP mice (both with and without Dox pre-treatment), but not in teto-hAPP controls or OMP-hAPP-$BACE^{(-/-)}$ mice (Figure 2a, b). These deposits resemble diffuse plaques (Figure 2a, b). Extracellular β-amyloid plaques were observed at the earliest time point (6-months) specifically in the glomerular layer of the OB in OMP-hAPP mice (Figure 2c). The β-amyloid plaques appeared within the granule cell layer by 12-months and progressively accumulated by 18- and 24-months (Figure 2d–f). RT-qPCR was used to confirm that expression of the hAPP gene was confined to the olfactory system (OE and OB) of OMP-hAPP animals and therefore the presence of β-amyloid deposits in downstream brain regions was not the result of aberrant expression of the transgene (Supplementary Figure S1). Stereological quantification of β-amyloid plaque load in the OB of OMP-hAPP mice using the area fraction fractionator probe showed a significant increase in the percentage volume of plaques with age from 6- to 12- to 18-months (Figure 2g, Supplementary Table S1 and S2). β-amyloid was observed in the AON and anterior piriform cortex by 18-months. By 24-months, plaque load had increased in these regions and progressed to the posterior piriform cortex and hippocampus (Figure 2h, Figure 3, Supplementary Figure S2, Supplementary Figure S4). Immunofluorescent triple labelling using three different β-amyloid antibodies confirmed that these plaques were comprised of β-amyloid (Supplementary Figure S3).

The OMP-hAPP Dox pre-treatment mice with delayed hAPP expression showed reduced β-amyloid plaque load in the OB at 18-months compared to the OMP-hAPP mice (Figure

2g, Supplementary Table S1 and S2) and qualitatively the distribution of plaques was similar to the 12-month OMP-hAPP mice (Figure 2h).

OB volume is reduced in OMP-hAPP mice

Comparison of gross OB volume indicated that OMP-hAPP mice had smaller OBs than teto-hAPP mice at all timepoints (Figure 4a). Stereological quantification showed that mean OB volume of OMP-hAPP mice was 38.1 ± 4.8% that of teto-hAPP mice at 6-months, 36.5 ± 4.9% at 12-months and 41.1 ± 6.8% at 18-months (Figure 4b, Supplementary Table S3 and S4). There was no significant difference in OMP-hAPP OB volume across the time points, indicating OB volume did not decline with age relative to controls. The 18-month OMP-hAPP Dox pre-treated mice had significantly larger OBs than the OMP-hAPP mice at all timepoints (Figure 4b, Supplementary Table S3 and S4).

For the AON, PIR and HP of OMP-hAPP mice there was no significant difference in region volume as a percentage of control between the different timepoints, nor was there a difference between OMP-hAPP mice and OMP-hAPP Dox pre-treated mice (Figure 4b, Supplementary Table S3 and S4).

Similarly, the OB volume of OMP-hAPP-BACE$^{(-/-)}$ mice was 35.9 ± 6.3% of teto-hAPP-BACE$^{(-/-)}$ mice at 6 months, 36.4 ± 10.7% at 12-months and 51.8 ± 8.6% at 18-months (Figure 4c, Supplementary Table S3 and S5). There was no significant difference in region volume for the OB, AON, PIR or HP across the timepoints.

Glomerular layer volume is reduced in OMP-hAPP mice

The glomerular layer of OMP-hAPP, OMP-hAPP Dox pre-treatment and OMP-hAPP-BACE$^{(-/-)}$ mice appeared thinner and the glomeruli were disorganized compared to their respective controls (Figure 5a–c). Using the Cavalieri estimator, we determined that glomerular layer volume as a percentage of total OB volume was significantly reduced in 18-month old OMP-hAPP, OMP-hAPP Dox pre-treated, and OMP-hAPP-BACE$^{(-/-)}$ mice compared to their respective controls (One-way ANOVA with Šídák's multiple comparisons test of pre-selected comparisons; mean OMP-hAPP: 9.97 ± 0.52% of total OB volume; mean teto-hAPP: 22.13 ± 2.8% of total OB volume; $P < 0.0001$. Mean OMP-hAPP Dox: 16.81 ± 1.35% of total OB volume; mean teto-hAPP Dox: 23.94 ± 2.1% of total OB volume; $P = 0.0001$. Mean OMP-hAPP-BACE$^{(-/-)}$: 13.82 ± 2.45% of total OB volume; mean teto-hAPP-BACE$^{(-/-)}$: 25.24 ± 1.6% of total OB volume; $P < 0.0001$. Figure 5d). Glomerular layer volume of OMP-hAPP mice was also significantly less than that of the OMP-hAPP Dox pre-treatment mice (One-way ANOVA with Šídák's multiple comparisons test, $P = 0.0002$).

OB development is impaired in OMP-hAPP mice

We used MEMRI to investigate whether the reduction in OB volume is due to degeneration or impaired development. The average OB volume of 3-week-old OMP-hAPP mice was significantly less than that of teto-hAPP mice, suggesting OB growth was impaired by weaning age (Figure 6a, Supplementary Table S6). The teto-hAPP animals showed a progressive increase in OB volume at 6 weeks and 32 weeks (8-months), followed by a

plateau between 32 weeks and 72 weeks. However, the OB volume of OMP-hAPP animals decreased between 3-week-old and 6-week-old groups and plateaued between 6-week, 32-week and 72-week-old groups (Figure 6a). This indicates that OB volume of OMP-hAPP animals did not decline during adulthood.

As OMP gene expression is activated during pre-natal development, the hAPP transgene is presumably expressed during this early stage of OB development in the OMP-hAPP mice. Therefore, to examine the effect of hAPP expression during adulthood, we carried out MEMRI scans every 6–8 weeks on OMP-hAPP mice pre-treated with Dox until weaning age. Withdrawal of the Dox treatment at weaning permits expression of the hAPP gene from 3-weeks-old. The OB volume of OMP-hAPP mice in this Dox pre-treatment group was smaller than that of the teto-hAPP controls at 6-weeks (Figure 6b), but larger than that of the OMP-hAPP animals without Dox pre-treatment (Figure 6a). OB volume of the OMP-hAPP Dox pre-treatment group was consistent until 32-weeks, and subsequently declined slowly until 65-weeks. The teto-hAPP Dox-treated control group showed a steady increase in OB volume until 46 weeks before plateau.

Qualitative inspection of the MEMRI scans for each group showed that OMP-hAPP mice had reduced OB length (horizontal plane), depth (sagittal plane) and height (coronal plane) at all ages compared to teto-hAPP controls (Figure 6c–d). The late onset OMP-hAPP Dox pre-treatment mice had reduced OB depth (sagittal plane) at 6 weeks old (Figure 6c) but appeared to have more reduced OB length (horizontal plane) and height (coronal plane) at 65-weeks-old (Figure 6d).

Discussion:

In this study we assessed the spread of β-amyloid from the OE to the OB and downstream connected brain regions. As olfactory deficits are an early symptom of AD, and β-amyloid and tau aggregates accumulate in the OB very early in the disease, the olfactory system may be an initial site of aggregate accumulation in the human disease. While a previous study has demonstrated the acute spread of β-amyloid injected directly into the OB over 72 hours, in human AD the process of β-amyloid accumulation is likely to be slow (He et al., 2018). Furthermore, the olfactory vector hypothesis implies that the olfactory sensory neurons would be the source of the β-amyloid rather than the OB. Our study is the first demonstration that APP expressed in the OE can lead to the passive spread of β-amyloid plaques to downstream brain regions over time.

Our results show that the β-amyloid plaques progressively accumulate in brain regions further downstream of the OE with age, and at each timepoint the density of plaques in these regions increased. This pattern of progressive plaque deposition from the OE to the OB, then piriform cortex and hippocampus agrees with previous studies where amyloid or alpha synuclein were injected directly into the bulb (Rey et al., 2016, 2019; He et al., 2018), but our study shows a slower pace of spread. We have inferred that the progressive appearance and increased density of β-amyloid labelling in these regions at subsequent time-points is indicative of β-amyloid movement from upstream regions. However, it should be considered that as different animals are studied at each timepoint, we are not

able to conclusively demonstrate this movement. The steady spread and accumulation of β-amyloid is highlighted by the Dox pre-treatment OMP-hAPP mice where hAPP expression is delayed. By 18-months of age, the plaque distribution in these Dox pre-treated mice more closely resembled the 12-month-old OMP-hAPP mice. However, quantitatively the plaque load in these regions resembled the 6-month-old OMP-hAPP mice. The more rapid accumulation of β-amyloid in the OMP-hAPP mice might reflect the prenatal production of hAPP in these animals, as the OMP promoter becomes active at embryonic day 14 (Graziadei et al., 1980). However, the conserved pattern of plaque progression in both the OMP-hAPP and the OMP-hAPP Dox pre-treated mice, suggests the mechanism of deposition from OE to OB is conserved regardless of when hAPP expression begins.

The distribution of β-amyloid within the OMP-hAPP olfactory system differs to that observed in the human AD OB. We observed β-amyloid plaques concentrated within the glomerular and granule cell layer in the OMP-hAPP mice, however in human AD, the density of plaques is higher in the AON than in these layers (Murray et al., 2020). This discrepancy highlights a key anatomical difference between rodent and human olfactory bulb anatomy. The AON is located within the olfactory bulb in humans while the rodent AON is situated posterior to the bulb. Therefore, the difference in β-amyloid distribution between the OMP-hAPP mice and that of human AD may reflect a fundamental difference in the anatomical route by which amyloid may spread along the olfactory pathway in humans and rodents.

Our design-based stereology analysis of OB volume showed that OMP-hAPP and OMP-hAPP-BACE$^{-/-}$ mice had reduced OB volume compared to controls. However, OB volume as a percentage of controls did not decline with age. This suggests the reduced OB volume is not due to degeneration. The reduced volume may instead reflect impaired OB growth due to pre-natal hAPP expression. To investigate this, we examined OB volume in OMP-hAPP Dox pre-treated mice, where the hAPP expression is delayed until 3-weeks old. At 18-months the OB volume of Dox pre-treatment mice was significantly less than controls but larger than the OMP-hAPP mice without Dox pre-treatment, indicating that delayed onset of the transgene expression had reduced the volume deficit.

To further confirm that the OB volume loss is due to impaired development rather than degeneration, we examined OB volume changes over time using MEMRI. This contrast technique highlights the laminar anatomy of the OB as previously described (Saar et al., 2015). By tracking the OB volume of each group over time it was evident that the OBs of OMP-hAPP mice are smaller than controls from the earliest time point we measured and do not grow over time. Similarly, the OB volume of Dox pre-treatment OMP-hAPP mice did not increase once the transgene was activated at weaning age. Overall, our results suggest that expression of hAPP in the OE leads to impaired OB growth rather than neurodegeneration.

Our results also showed that reduced glomerular layer volume is a contributing factor to the overall reduction of OB volume in OMP-hAPP mice. Previous studies using the OMP-hAPP mice show apoptosis of OSNs occurs by 3 weeks of age as well as distortion of glomerular structure and loss of OSN axonal convergence (Cheng et al., 2013). Loss of OSNs leads to

loss of sensory input which is necessary for postnatal OB growth as studies of unilateral naris occlusion at birth show that OB volume is reduced on the occluded side while the open side develops normally (Cummings et al., 1997; Pothayee et al., 2017). Therefore, the reduced OB volume is likely due to a loss of OSN input from the onset of hAPP expression, which prevents OB growth. As this loss of glomerular input occurs before plaques form in the OB, and the OMP-hAPP-BACE$^{(-/-)}$ mice also show reduced glomerular layer volume, we conclude that the glomerular distortion is independent of β-amyloid plaque production, which agrees with previous findings(Cao et al., 2012b; Cheng et al., 2016). Therefore, it is likely that loss of glomerular input is caused by mutant hAPP(sw,ind) or other hAPP cleavage products. Previous studies of this OMP-hAPP model demonstrate that expression of hAPP(sw,ind) causes OSN death via the caspase-9-mediated intrinsic apoptosis pathway(Cheng et al., 2016). Based on this data, we propose that apoptosis of OSNs caused by hAPP expression leads to reduced sensory input and impaired OB growth.

Reduced glomerular volume has functional consequences as previously demonstrated. OMP-hAPP mice show impaired odour detection and discrimination compared to controls and OSN loss is correlated with deficits in olfactory performance (Cao et al., 2012b; Cheng et al., 2013). In-vivo functional imaging also shows reduced strength of the OSN-glomeruli synapse (Cheng et al., 2013). These previous studies examined OMP-hAPP mice at 3 weeks and 3–5 months, so additional behavioural studies would be required to assess whether the functional deficit increases with older mice. Overall, our results align with previous studies to conclude that OSNs are either sensitive to elevated hAPP levels or the familial AD hAPP mutations impair OSN function.

Reduced glomerular volume due to OSN loss is also relevant to the human OB. A recent study of the OB in human AD shows a significant reduction in glomerular layer volume and elevated β-amyloid and microgliosis, particularly on the ventral side of the OB (Son et al., 2022). Their analysis indicated that the glomerular layer shrinkage was due to glomeruli atrophy rather than a reduced number of glomeruli. In agreement with our data, we propose the reduced glomerular volume in human AD is likely due to the loss of OSN axons or disrupted axon targeting rather than bulbar degeneration. The accumulation of β-amyloid specifically in the ventral glomerular layer of the human AD OB is likely due to deposition by the OSNs as we observed in the OMP-hAPP mice. Altered glomeruli morphology could also be due to loss of OSN input. The distorted and irregular shape of glomeruli in the human bulb, even in older neurologically normal individuals, may arise from the combination of OSN loss and axon retargeting over a lifetime (Murray et al., 2022; Son et al., 2022). We observed the glomeruli in OMP-hAPP mice to have a similar distorted shape while control mice have a more consistent spherical morphology. As we observed loss of glomerular layer volume in OMP-hAPP-BACE(−/−) mice independent of plaques, it is plausible that peri-glomerular β-amyloid accumulation in human AD is not the direct cause of the glomerular alterations.

The delayed appearance of β-amyloid plaques in the OB of Dox pre-treated animals may reflect the more mature state of the OB when hAPP expression begins. During early postnatal development OSN axons gradually refine their precise targeting to the OB while undergoing continuous turnover in the OE. This refinement process may result in greater

levels of β-amyloid deposits in the OB as new axons are introduced to establish an accurate olfactory bulb map. Once the OB matures and axonal refinement is complete, β-amyloid deposits may accumulate at a reduced rate. Consistent with this we find that developmental axon targeting is less disrupted when the OSN hAPP expression is delayed. A previous study using the OMP-hAPP model shows that early hAPP overexpression causes OSN axons to mistarget and innervate many glomeruli rather than one (Cheng et al., 2013). Therefore, delaying hAPP expression may result in a less extensive innervation of OSN axons that contain hAPP entering the OB and thus a slower accumulation of β-amyloid plaques. While APP presumably does not accumulate in human OSNs during development, remodelling of the OE may occur in response to external insults such as injury, infection, or exposure to toxins. In such a case, OSNs would regenerate as BACE1 is upregulated in response to injury (Cole and Vassar, 2007) and facilitate remodelling through cleavage of axon guidance proteins (Rajapaksha et al., 2011; Cao et al., 2012a). Therefore, an injury to the OE during adult life could also lead to increased BACE1 expression, subsequent APP cleavage and gradual accumulation of β-amyloid within OSNs that target to the OB and slowly spread to downstream brain regions in human Alzheimer's disease.

Lastly, we found that the volume of downstream brain regions (AON, PIR, HP) was not altered in OMP-hAPP or OMP-hAPP-BACE$^{(-/-)}$ mice at any timepoint, despite plaques forming in the AON and PIR of OMP-hAPP mice by 18-months. This further supports the conclusion that plaque accumulation and impaired OB growth does not directly affect the gross anatomy of these regions. A more detailed assessment of neuron number using stereology would be needed to detect more subtle differences. However, our results align with previous evidence showing that β-amyloid alone does not cause cortical atrophy in vivo (Jankowsky and Zheng, 2017).

Overall, our results suggest that olfactory dysfunction in Alzheimer's disease is unlikely to be solely due to β-amyloid-induced degeneration. From current literature it is unclear whether human OB volume is reduced in Alzheimer's disease (Jobin et al., 2021). Several MRI studies that measured the human OB and olfactory tract reported reduced volume in Alzheimer's disease patients (Thomann et al., 2009b, 2009a; Petekkaya et al., 2020), while an additional study reported no difference in volume when the OB alone was measured (Servello et al., 2015). These studies are limited by the resolution of clinical MRI relative to the very small size of the human OB, together with small sample sizes and large inter-individual variability in human OB volume. Therefore, it is currently unclear whether OB degeneration is a feature of human Alzheimer's disease and if not, then the absence of degeneration in the Dox- pre-treated OMP-hAPP mice is perhaps not unexpected.

In conclusion, this study provides evidence that β-amyloid produced by OSN expression of hAPP can spread to the hippocampus via the OB. These results support an olfactory route of β-amyloid spread and accumulation and highlight the potential involvement of the olfactory system in the earliest stages of in Alzheimer's disease.

Methods:

Transgenic Lines

All animal experiments were performed in accordance with the NIH guidelines and were approved by the Animal Care and Use Committee of the National Institute of Neurological Disorder and Stroke, National Institutes of Health (Bethesda, MD USA). Reporting in this manuscript follows the recommendations in the ARRIVE guidelines(du Sert et al., 2020).

The OMP-hAPP line was bred by crossing the TetO-hAPP line containing the hAPP transgene with familial AD mutations KM570, 571NL “Swedish” and V617F “Indiana” (RRID: MMRRC_034846-MU) with the OMP-tTA line (RRID: IMSR_JAX:017754) that expresses the tTA in mature OSNs (Yu et al., 2004; Jankowsky et al., 2005; Nguyen et al., 2007). The expression of hAPP by the OSNs presumably begins when the OMP promoter is activated during embryonic development. OMP-hAPP animals were confirmed by genotyping. Littermates with only the tetO-hAPP transgene or the OMP-tTA transgene were examined and the results were indistinguishable as previously described (Cheng et al., 2016). In most cases, littermates with the tetO-hAPP transgene were selected as controls. The OMP-hAPP animals were crossed with a null β-site APP cleaving enzyme 1 ($BACE^{-/-}$) line (RRID: IMSR_JAX:004714) to generate OMP-hAPP-$BACE^{+/-}$ and OMP-hAPP-$BACE^{-/-}$ lines as previously described (Cheng et al., 2016). All mice were of mixed (129 × C57BL/6) background and both sexes were used in the study.

For the study of late-onset hAPP expression, Dox-containing chow (6 g/kg, 0.5-inch pellets, Bio-Serv, Frenchtown, NJ) was fed to lactating mothers until the pups were weaned at 2- to 3-weeks old. Dox prevents the tTA-protein from binding to the tetO-sequence, thereby preventing the expression of hAPP until weaning age.

PCR genotyping

The following PCR primers were used for genotyping: OMP-tTA: 5’ GGTTGCGTATTGGAAGATCAAGAGC 3’; 5’ GAG-GAGCAGCTAGAAGAATGTCCC 3’; tetO-hAPP: 5’ CCGAGATCTCTGAAGTGAAGATGGATG 3’; 5’ CCAAGC-CTAGACCACGAGAATGC 3’; BACE: 5’ AGG CAG CTT TGT GGA GAT GGTG3’ (wild type); 5’ CGGGAAATGGAAAGGCTACTCC 3’ (common); and 5’ TGG ATG TGG AAT GTG TGC GAG 3’ (mutant) as described previously (Cheng et al., 2016).

Validation of hAPP mRNA expression

RT-qPCR was used to confirm that hAPP mRNA was not expressed in the hippocampus of OMP-hAPP animals. 18-month-old OMP-hAPP animals and their teto-hAPP littermates were euthanized and whole brains were removed from the skull and stored in RNALater (Sigma-Aldrich) at −20°C. Skulls with nasal epithelium intact were stored whole in RNALater (Sigma-Aldrich) at −20°C. 12-month-old C57BL/6J mice were euthanized, whole brains were removed from the skull, and one hemisphere was flash-frozen and stored at −80°C. Human tissue was obtained from the Neurological Foundation Human Brain Bank at the University of Auckland, New Zealand. The tissue was donated with informed consent from the family before brain removal, and all procedures were approved by the

University of Auckland Human Participants Ethics Committee (Ref: 011654). Total RNA was isolated from micro-dissected olfactory bulb, AON, hippocampus, and nasal epithelium of OMP-hAPP and teto-hAPP mouse brains, olfactory bulb of C57BL/6J mouse brains, and middle temporal gyrus of human Alzheimer's disease brains using the RNeasy Mini Kit (QIAGEN) following the manufacturer's instructions for tissue samples. The purity (OD260/280) and concentration of total RNA was analyzed using spectrophotometry (NanoDrop 1000, Thermo Fisher). Total RNA was diluted to a concentration of 20 ng/μl prior to cDNA synthesis to ensure that RNA input was consistent across samples. RNA was stored at −80°C until use. For cDNA synthesis, the High-Capacity RNA-to-cDNA Kit (Applied Biosystems) was used according to manufacturer's instructions. RT-qPCR was performed using SYBR Green RT-qPCR SuperMix-UDG with Rox (Life Technologies) as per previously published methods(Highet et al., 2021) and run on a QuantStudio 12K Flex machine (Applied Biosystems). CT was determined automatically using QuantStudio 12K Flex Software v.1.3. Primers were designed to be specific to either human or mouse *APP* in the expectation that OMP-hAPP mice would express both human and mouse *APP* in the olfactory system, while teto-APP mice would only express mouse *APP.* Details for the primers used in this study are available in Table 1.

Manganese-enhanced MRI (MEMRI)

100 mM of isotonic $MnCl_2$ (Sigma-Aldrich) solution was infused into the tail vein using a syringe pump (Cole-Parmer Instrument) at a dose of 88 mg/kg and an infusion rate of 0.25 ml/h (total infusion time of ~20 min). During the infusion, mice were anesthetized with 1–2% isoflurane (1:4 air:oxygen mixture) and their body temperature was maintained by a heated water pad. After infusion, mice were returned to the cage and were monitored until fully awake. No abnormalities were observed after infusion in all mice. MRI scanning was performed 24 h after manganese administration. Animals were anesthetized with 1.2–2% isoflurane using a nose cone, and their body temperature maintained at 37 °C by a heated water bath.

Images were acquired on an 11.7 T/31 cm horizontal bore magnet (Agilent, Oxford, UK), interfaced to an Avance III console (Bruker Biospin, Billerica, MA). A custom built 9 cm diameter birdcage coil was used for homogeneous RF transmission and a small surface coil, 6 mm in diameter, placed in the area of the OB, was used during acquisition. Each animal from the Dox pre-treatment group was imaged every 4–10 weeks between the ages of 6–65 weeks and sacrificed after the final scan. For the OMP-hAPP animals without Dox pre-treatment, scans were performed on cohorts of animals at ages of 3, 6, 32 and 72 weeks prior to sacrifice (Figure 1c).

Manganese enhanced MRI (MEMRI) images were acquired using a 3D T_1 weighted fast low angle shot (FLASH) sequence, at 50 μm isotropic resolution, with TR/TE = 40/4.4 ms, 25° pulse, and bandwidth = 50 kHz. At early ages (< 20 weeks): FOV = 12.8 × 12.8 × 7.4 mm^3, matrix size = 256 × 256 × 148, number of averages = 2, and total scan time of 50 min. At later ages: FOV = 16 × 12.8 × 7.5 mm3, matrix size = 320 × 256 × 150, number of averages = 3, and total scan time of 1h 25 min.

MRI analysis

The OB volume was measured using Medical Image Processing, Analysis, and Visualization (MIPAV) software (NIH; http://mipav.cit.nih.gov). Both bulbs were manually segmented, and the total bulb volume measured. Measurements are presented as average bulb volume ± standard deviation (SD) per group.

Tissue Processing

Mice were anesthetized with isoflurane and transcardially perfused with 1x phosphate-buffered saline followed by 4% PFA. The brains were removed, post-fixed, embedded in 10% gelatin + 0.1M phosphate buffer and cryoprotected in 2% PFA + 10% sucrose overnight, then 30% sucrose overnight. The blocks were subsequently snap frozen in chilled isopentane and stored at −80°C prior to sectioning. The blocks were embedded in O.C.T. freezing medium (Tissue-Tek) and coronally sectioned at 50 μm thickness on a cryostat at −18°C. The sections were stored at −80°C prior to immunohistochemistry.

Fluorescent Immunohistochemistry and microscopy

A 1:6 series of sections were fluorescently labelled for stereological quantification of region of interest (ROI) volume. At least five mice per group were used per time point. Sample size was determined based on previous publications (Cheng et al., 2011, 2016; Saar et al., 2015) and loss of animals with aging. No animals from any group were excluded from the analysis. Immunohistochemistry was performed as previously described (Cummings and Belluscio, 2010; Saar et al., 2015; Cheng et al., 2016). Primary antibodies included: mouse anti-beta amyloid diluted 1:100 (6E10, Biolegend 803002, reactivity with Human beta amyloid, RRID: AB_2564654), goat anti-OMP diluted 1:1000 (WAKO 019-22291, RRID: AB_664696) and rabbit anti-NeuN diluted 1:500 (Millipore ABN78, RRID: AB_10807945) in immunobuffer (3% horse serum, 0.2% triton in tris-buffered saline). Secondary antibodies were diluted 1:600 in immunobuffer: donkey anti-rabbit Alexa Fluor 488 (Jackson Lab 711-545-152), donkey anti mouse cy3 (Jackson Lab 715-165-150) and donkey anti-goat Alexa Fluor 647 (Jackson lab 705-605-147). Stitched images of the full tissue sections were obtained using a Zeiss LSM800 confocal microscope with a 10x objective.

Stereological Quantification

Estimation of ROI volume and percentage volume of β-amyloid plaques was obtained using the Area Fraction Fractionator probe within the StereoInvestigator software (MBF Bioscience). The whole section stitched confocal images were imported into the StereoInvestigator software. Contours for the ROIs (OB, AON, PIR and HP) were manually drawn according to the Allen Mouse Brain Atlas (©2011 Allen Institute for Brain Science. Allen Mouse Brain Atlas) Available from: mouse.brain-map.org (Lein et al., 2007). We used a 300 × 300 μm sampling grid with a 150 × 150 μm^2 counting frame and 20 μm marker spacing. At each predetermined site, one type of marker was placed over β-amyloid plaques and a different marker was placed over the rest of the tissue area. The process was repeated until all sites were quantified. The output is an estimate of total ROI volume and percentage of the total ROI volume containing β-amyloid plaques. The ROI volume of OMP-hAPP

mice was normalized to the average ROI volume for teto-hAPP control mice at the same time-point.

Estimation of glomerular layer volume was obtained using the Cavalieri estimator. A contour was manually drawn around the glomerular layer and a 35 × 35 μm^2 grid was superimposed on the OB images. The grid points that fell within the contour were counted with a marker and the marker count was used to determine the glomerular layer volume across the OB sections per case. The glomerular layer volume for each case was normalized to the total OB volume that was determined using the Area Fraction Fractionator probe described above.

Statistical Analysis

The data were analyzed using GraphPad Prism version 9. The stereological plaque load and volume estimates for each ROI were compared between OMP-hAPP mice at different time points using a one-way ANOVA with Tukey multiple comparisons t-test. The plaque load estimates were compared between OMP-hAPP and control animals at each time point using a Mann-Whitney test as the data did not fit the assumption of normal distribution. The ROI volume estimates were compared between OMP-hAPP and control animals at each time point using an unpaired t-test as the data fit the assumptions of normal distribution and equality of variance. The MEMRI OB volume measurements for OMP-hAPP mice and OMP-hAPP Dox pre-treatment mice were compared to control mice at each time point using an unpaired t-test where the data fit the assumptions of normal distribution and equality of variance. If the data did not satisfy these assumptions, then a non-parametric Mann-Whitney U test was performed. Values are reported as mean ± standard deviation. Statistical significance was set as $P = 0.05$.

Supplementary Material

Refer to Web version on PubMed Central for supplementary material.

Acknowledgements

This research was supported by the Intramural Research Program of the NIH, NINDS.

H.C.M is a Heath Education Trust Postdoctoral Research Fellow, and this research was funded by the Health Education Trust.

Data Availability

The image data used for this study is available from the corresponding author on reasonable request. All other data generated or analysed during this study are included in this published article (and its Supplementary Information files).

Abbreviations:

OE	olfactory epithelium
OMP	olfactory marker protein

hAPP	humanized amyloid precursor protein
BACE	β-site APP cleaving enzyme 1
SD	standard deviation
ROI	region of interest
OB	olfactory bulb
OMP	olfactory marker protein
AON	anterior olfactory nucleus
PIR	piriform cortex
HP	hippocampus
Dox	doxycycline

References

Arnold SE, Lee EB, Moberg PJ, Stutzbach L, Kazi H, Han L-Y, Lee VMY, Trojanowski JQ (2010) Olfactory epithelium amyloid-β and paired helical filament-tau pathology in Alzheimer disease. Ann Neurol 67:462–469 Available at: http://doi.wiley.com/10.1002/ana.21910. [PubMed: 20437581]

Attems J, Lintner F, Jellinger KA (2005) Olfactory involvement in aging and Alzheimer's disease: An autopsy study. Journal of Alzheimer's Disease 7:149–157 Available at: http://www.ncbi.nlm.nih.gov/pubmed/15851853.

Braak H, Braak E (1995) Staging of Alzheimer's disease-related neurofibrillary changes. Neurobiol Aging 16:271–278; discussion 278–84 Available at: http://www.sciencedirect.com/science/article/pii/0197458095000216. [PubMed: 7566337]

Cao L, Rickenbacher GT, Rodriguez S, Moulia TW, Albers MW (2012a) The precision of axon targeting of mouse olfactory sensory neurons requires the BACE1 protease. Sci Rep 2:1–8.

Cao L, Schrank BR, Rodriguez S, Benz EG, Moulia TW, Rickenbacher GT, Gomez AC, Levites Y, Edwards SR, Golde TE, Hyman BT, Barnea G, Albers MW (2012b) Aβ 2 alters the connectivity of olfactory neurons in the absence of amyloid plaques in vivo. Nat Commun 3.

Cheng N, Bai L, Steuer E, Belluscio L (2013) Olfactory functions scale with circuit restoration in a rapidly reversible Alzheimer's disease model. J Neurosci 33:12208–12217 Available at: http://www.ncbi.nlm.nih.gov/pubmed/23884929. [PubMed: 23884929]

Cheng N, Cai H, Belluscio L (2011) In vivo olfactory model of APP-induced neurodegeneration reveals a reversible cell-autonomous function. J Neurosci 31:13699–13704 Available at: https://www.ncbi.nlm.nih.gov/pmc/articles/PMC3190161/pdf/nihms328310.pdf. [PubMed: 21957232]

Cheng N, Jiao S, Gumaste A, Bai L, Belluscio L (2016) APP Overexpression Causes Aβ-Independent Neuronal Death through Intrinsic Apoptosis Pathway. eNeuro 3 Available at: http://eneuro.sfn.org/cgi/doi/10.1523/ENEURO.0150-16.2016.

Cole SL, Vassar R (2007) The Alzheimer's disease β-secretase enzyme, BACE1. Mol Neurodegener 2:1–25. [PubMed: 17224059]

Cummings DM, Belluscio L (2010) Continuous neural plasticity in the olfactory intrabulbar circuitry. Journal of Neuroscience 30:9172–9180. [PubMed: 20610751]

Cummings DM, Henning HE, Brunjes PC (1997) Olfactory Bulb Recovery after Early Sensory Deprivation.

Dando SJ, Mackay-Sim A, Norton R, Currie BJ, st. John JA, Ekberg JAK, Batzloff M, Ulett GC, Beacham IR (2014) Pathogens penetrating the central nervous system: Infection pathways and the cellular and molecular mechanisms of invasion. Clin Microbiol Rev 27:691–726.

Devanand DP, Michaels-Marston KS, Liu X, Pelton GH, Padilla M, Marder K, Bell K, Stern Y, Mayeux R (2000) Olfactory deficits in patients with mild cognitive impairment predict Alzheimer's disease at follow-up. Am J Psychiatry 157:1399–1405 Available at: http://www.ncbi.nlm.nih.gov/pubmed/10964854. [PubMed: 10964854]

Doty RL (2008) The olfactory vector hypothesis of neurodegenerative disease: Is it viable? Ann Neurol 63:7–15. [PubMed: 18232016]

du Sert NP et al. (2020) Reporting animal research: Explanation and elaboration for the arrive guidelines 2.0.

Graziadei GAM, Stanley RS, Graziadei PPC (1980) The olfactory marker protein in the olfactory system of the mouse during development. Neuroscience 5:1239–1252. [PubMed: 7402467]

He B, Zheng M, Liu Q, Shi Z, Long S, Lu X, Pei Z, Yuan TF, Su H, Yao X (2018) Injected Amyloid Beta in the Olfactory Bulb Transfers to Other Brain Regions via Neural Connections in Mice. Mol Neurobiol 55:1703–1713. [PubMed: 28211008]

Highet B, Parker R, Faull RLM, Curtis MA, Ryan B (2021) RNA Quality in Post-mortem Human Brain Tissue Is Affected by Alzheimer's Disease. Front Mol Neurosci 14:1–8.

Jankowsky JL, Slunt HH, Gonzales V, Savonenko A v., Wen JC, Jenkins NA, Copeland NG, Younkin LH, Lester HA, Younkin SG, Borchelt DR (2005) Persistent amyloidosis following suppression of Aβ production in a transgenic model of Alzheimer disease. PLoS Med 2:1318–1333.

Jankowsky JL, Zheng H (2017) Practical considerations for choosing a mouse model of Alzheimer's disease. Mol Neurodegener 12:1–22. [PubMed: 28049533]

Jobin B, Boller B, Frasnelli J (2021) Volumetry of olfactory structures in mild cognitiveimpairment and alzheimer's disease: A systematic review and a meta-analysis. Brain Sci 11:1–16.

Koo EH, Sisodia SS, Archer DR, Martin LJ, Weidemann A, Beyreuther K, Fischer P, Masters CL, Price DL (1990) Precursor of amyloid protein in Alzheimer disease undergoes fast anterograde axonal transport. Proc Natl Acad Sci U S A 87:1561–1565. [PubMed: 1689489]

Kovács T, Cairns NJ, Lantos PL (2001) Olfactory centres in Alzheimer's disease: olfactory bulb is involved in early Braak's stages. Neuroreport 12:285–288 Available at: http://www.ncbi.nlm.nih.gov/pubmed/11209936. [PubMed: 11209936]

Lein ES et al. (2007) Genome-wide atlas of gene expression in the adult mouse brain. Nature 445:168–176. [PubMed: 17151600]

Morales R, Callegari K, Soto C (2015) Prion-like features of misfolded Aβ and tau aggregates. Virus Res 207:106–112 Available at: 10.1016/j.virusres.2014.12.031. [PubMed: 25575736]

Murray HC, Dieriks BV, Swanson ME v, Anekal PV, Turner C, Faull RLM, Belluscio L, Koretsky A, Curtis MA (2020) The unfolded protein response is activated in the olfactory system in Alzheimer's disease. Acta Neuropathol Commun 8:109 Available at: https://actaneurocomms.biomedcentral.com/articles/10.1186/s40478-020-00986-7. [PubMed: 32665027]

Murray HC, Johnson K, Sedlock A, Highet B, Dieriks BV, Anekal PV, Faull RLM, Curtis MA, Koretsky A, Maric D (2022) Lamina-specific immunohistochemical signatures in the olfactory bulb of healthy, Alzheimer's and Parkinson's disease patients. Commun Biol 5:88 Available at: https://www.nature.com/articles/s42003-022-03032-5. [PubMed: 35075270]

Nguyen MQ, Zhou Z, Marks CA, Ryba NJP, Belluscio L (2007) Prominent Roles for Odorant Receptor Coding Sequences in Allelic Exclusion. Cell 131:1009–1017. [PubMed: 18045541]

Olsson TT, Klementieva O, Gouras GK (2018) Neurobiology of Disease Prion-like seeding and nucleation of intracellular amyloid-β. Neurobiol Dis 113:1–10 Available at: 10.1016/j.nbd.2018.01.015. [PubMed: 29414379]

Petekkaya E, Kaptan Z, Unalmis D, Burakgazi G (2020) An investigation of olfactory bulb and entorhinal cortex volumes in both patients with Alzheimer's disease and healthy individuals, and a comparative analysis of neuropeptides. 9:866–871.

Pothayee N, Cummings DM, Schoenfeld TJ, Dodd S, Cameron HA, Belluscio L, Koretsky AP (2017) Magnetic resonance imaging of odorant activity-dependent migration of neural precursor cells and olfactory bulb growth. Neuroimage 158:232–241 Available at: 10.1016/j.neuroimage.2017.06.060. [PubMed: 28669915]

Rajapaksha TW, Eimer WA, Bozza TC, Vassar R (2011) The Alzheimer's b-secretase enzyme BACE1 is required for accurate axon guidance of olfactory sensory neurons and normal

glomerulus formation in the olfactory bulb. Mol Neurodegener 6 Available at: http://www.molecularneurodegeneration.com/content/6/1/88.

Rey NL, Bousset L, George S, Madaj Z, Meyerdirk L, Schulz E, Steiner JA, Melki R, Brundin P (2019) α-Synuclein conformational strains spread, seed and target neuronal cells differentially after injection into the olfactory bulb. Acta Neuropathol Commun 7:221 Available at: https://actaneurocomms.biomedcentral.com/articles/10.1186/s40478-019-0859-3. [PubMed: 31888771]

Rey NL, Steiner JA, Maroof N, Luk KC, Madaj Z, Trojanowski JQ, Lee VM-Y, Brundin P (2016) Widespread transneuronal propagation of α-synucleinopathy triggered in olfactory bulb mimics prodromal Parkinson's disease. J Exp Med 213:1759–1778. [PubMed: 27503075]

Rey NL, Wesson DW, Brundin P (2018) The olfactory bulb as the entry site for prion-like propagation in neurodegenerative diseases. Neurobiol Dis 109:226–248 Available at: http://www.ncbi.nlm.nih.gov/pubmed/28011307. [PubMed: 28011307]

Saar G, Cheng N, Belluscio L, Koretsky AP (2015) Laminar specific detection of APP induced neurodegeneration and recovery using MEMRI in an olfactory based Alzheimer's disease mouse model. Neuroimage 118:183–192. [PubMed: 26021215]

Servello A, Fioretti A, Gualdi G, di Biasi C, Pittalis A, Sollaku S, Pavaci S, Tortorella F, Fusetti M, Valenti M, Masedu F, Cacciafesta M, Marigliano V, Ettorre E, Pagliarella M (2015) Olfactory Dysfunction, Olfactory Bulb Volume and Alzheimer's Disease: Is There a Correlation? A Pilot Study. Journal of Alzheimer's Disease 48:395–402.

Son G M, Steinbusch HW, López-Iglesias C, Moon C, Jahanshahi A, Ali Jahanshahi C (2022) Severe histomorphological alterations in post-mortem olfactory glomeruli in Alzheimer's disease. Brain Pathology 32:13033 Available at: 10.1111/bpa.13033.

Thal DR, Rüb U, Orantes M, Braak H (2002) Phases of Aβ-deposition in the human brain and its relevance for the development of AD. Neurology 58:1791–1800. [PubMed: 12084879]

Thomann PA, dos Santos V, Seidl U, Toro P, Essig M, Schröder J, Schröder S (2009a) MRI-Derived Atrophy of the Olfactory Bulb and Tract in Mild Cognitive Impairment and Alzheimer's Disease. Journal of Alzheimer's Disease 17:213–221.

Thomann PA, dos Santos V, Toro P, Schönknecht P, Essig M, Schröder J (2009b) Reduced olfactory bulb and tract volume in early Alzheimer's disease-A MRI study. Neurobiol Aging 30:838–841. [PubMed: 17875348]

Walker LC (2018) Prion-like mechanisms in Alzheimer disease. Handb Clin Neurol 153:303–319 Available at: 10.1016/B978-0-444-63945-5.00016-7. [PubMed: 29887142]

Yu CR, Power J, Barnea G, O'Donnell S, Brown HEV, Osborne J, Axel R, Gogos JA (2004) Spontaneous neural activity is required for the establishment and maintenance of the olfactory sensory map. Neuron 42:553–566. [PubMed: 15157418]

Highlights

- Spread of β-amyloid from olfactory sensory neurons to the olfactory bulb with age
- Reduced olfactory bulb volume due to APP-mediated disruption of development
- Progressive spread of β-amyloid to the piriform cortex and hippocampus
- β-amyloid deposition was not accompanied by regional atrophy

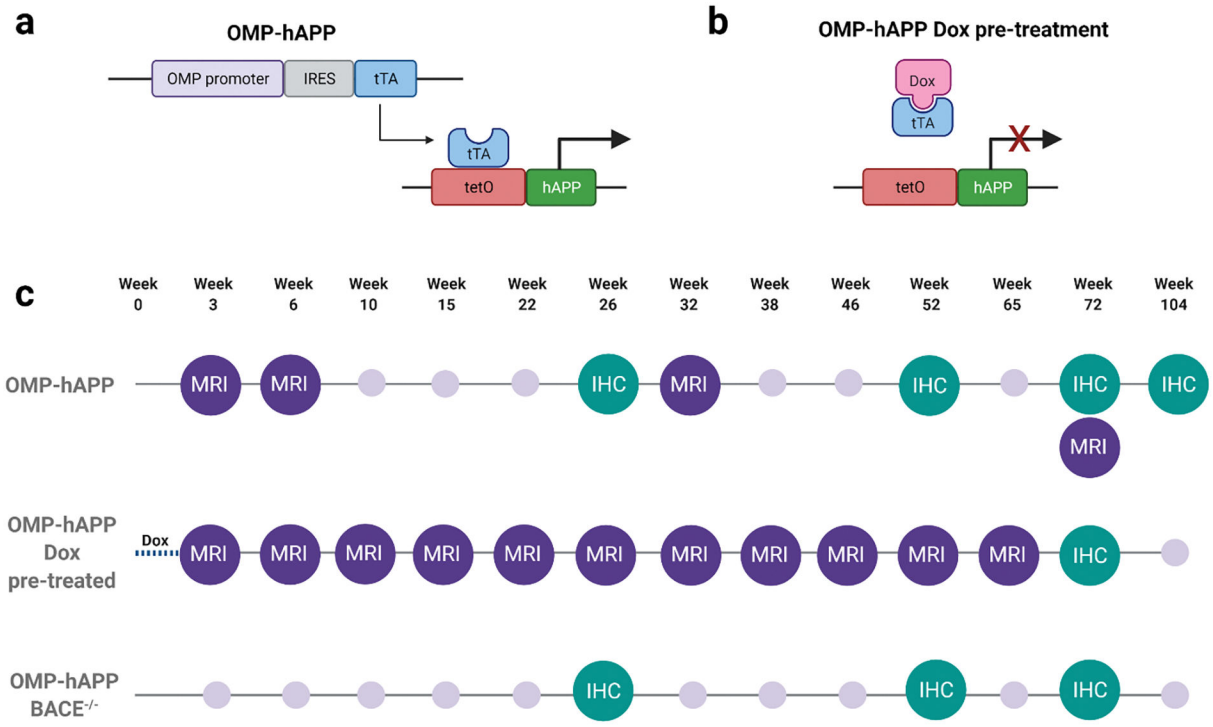

Figure 1. Schematic of the OMP-hAPP transgenic mice and timeline of experiments.

(a) The OMP-tTa and teto-hAPP lines were crossed to generate OMP-hAPP mice. hAPP expression is controlled by tTA under the OMP promoter, which is activated in mature OSNs. (b) In this tet-off system, when Dox is administered the expression of hAPP is turned off. For the OMP-hAPP Dox-pre-treatment group, this system was used to delay hAPP expression until mice were 3-weeks old. (c) Timeline of MRI and brain collection for immunohistochemistry each line. Note that for OMP-hAPP and OMP-hAPP-BACE$^{(-/-)}$ lines, different groups of animals were studied at each timepoint. For the OMP-hAPP Dox pre-treatment group, the same animals were scanned at each timepoint. Created with BioRender.com

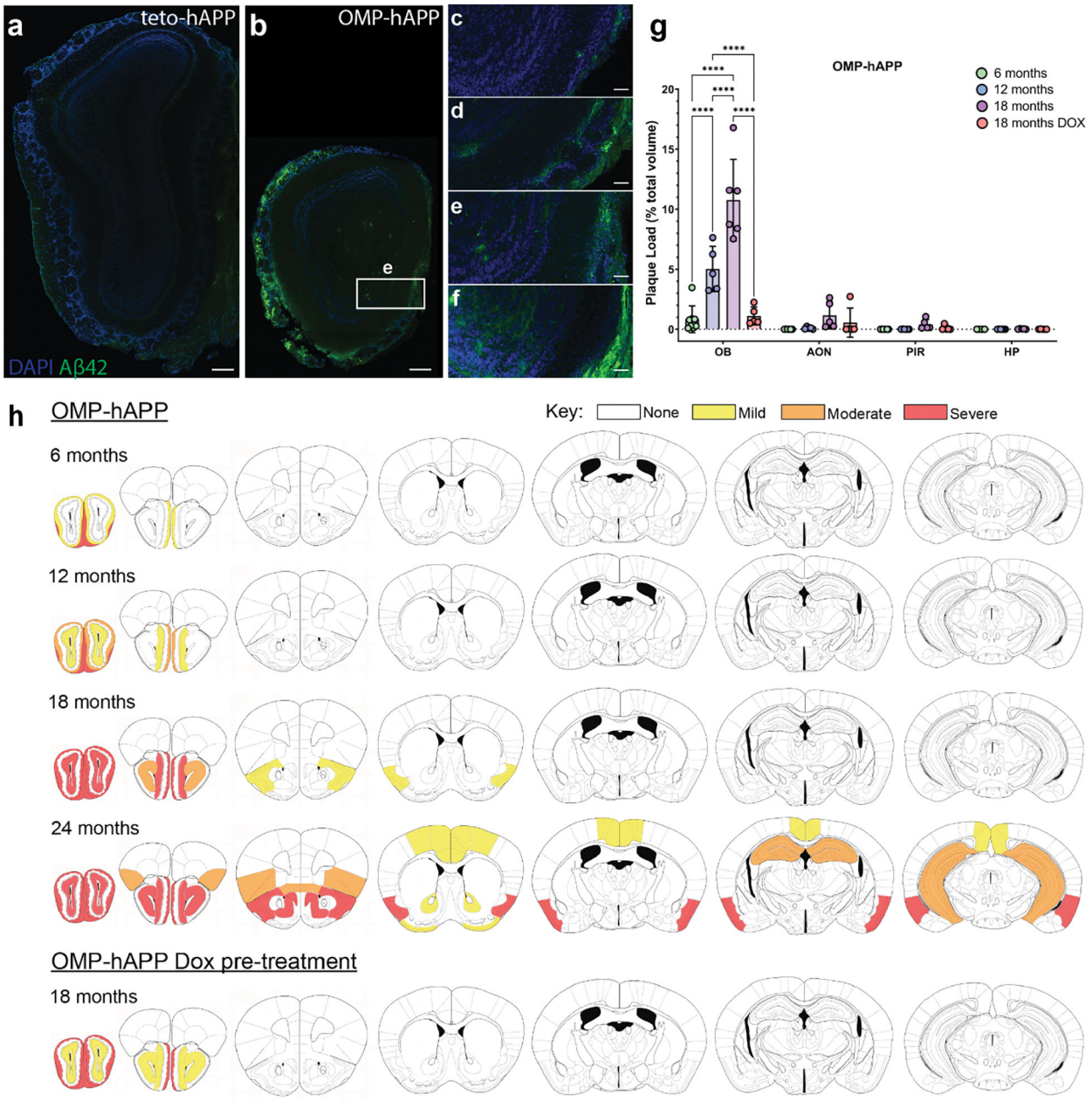

Figure 2. Progression of amyloid pathology along the olfactory pathway with age.

(a-b) Representative images of coronal OB sections from an 18-month teto-hAPP and OMP-hAPP animal labelled for DAPI (blue) and β-amyloid (green) illustrating diffuse plaques in the granule cell layer and glomerular layer in OMP-hAPP animals only. (c-f) β-amyloid accumulation in the OB at 6 (c), 12 (d), 18 (e) and 24-months (f). (g) Interleaved scatter with bars plot of plaque load in each ROI at 6-, 12- and 18-month-old OMP-hAPP animals and 18-month-old OMP-hAPP Dox pre-treated animals. Plaque load is expressed as percent of total volume for each region of interest, as determined using the area fraction fractionator probe of the StereoInvestigator software. Points represent individual animals, bars represent mean ± SD. $P \leq 0.0001$ for all statistically significant results (****). See Supplementary Table S1 for data on plaque load for each ROI and animal group. (h)

Schematic representation of plaque distribution on coronal sections at 6-, 12-, 18- and 24-month-old OMP-hAPP animals and 18-month-old OMP-hAPP Dox pre-treated animals. Examples of labelling classified as mild, moderate and severe is presented in Supplementary Figure S4. Abbreviations: olfactory bulb, OB; anterior olfactory nucleus, AON; piriform cortex, PIR; hippocampus, HP. Scale bars (a-b) 200 μm, (c-f) 50 μm.

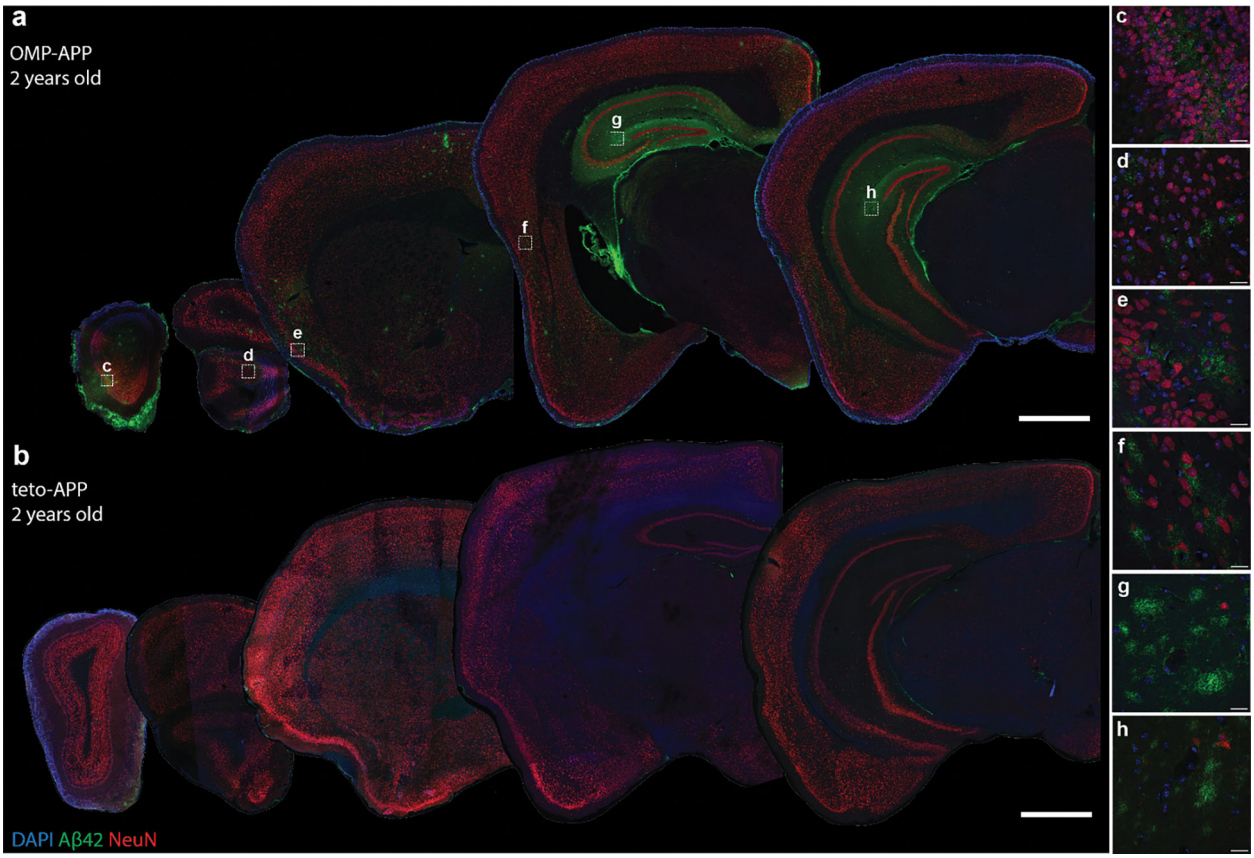

Figure 3. Distribution of amyloid pathology in 2-year-old OMP-hAPP mice.

A coronal series throughout the brain of a representative 2-year-old OMP-hAPP mouse (a) and teto-hAPP control littermate (b). High magnification images of the β-amyloid labelling in the OB (c), AON (d), piriform cortex (e-f), and hippocampus (g-h). The sections were labelled for DAPI (blue), β-amyloid (Aβ42, green) and NeuN (red). Scale bars 1 mm (a-b), 20 μm (c-h).

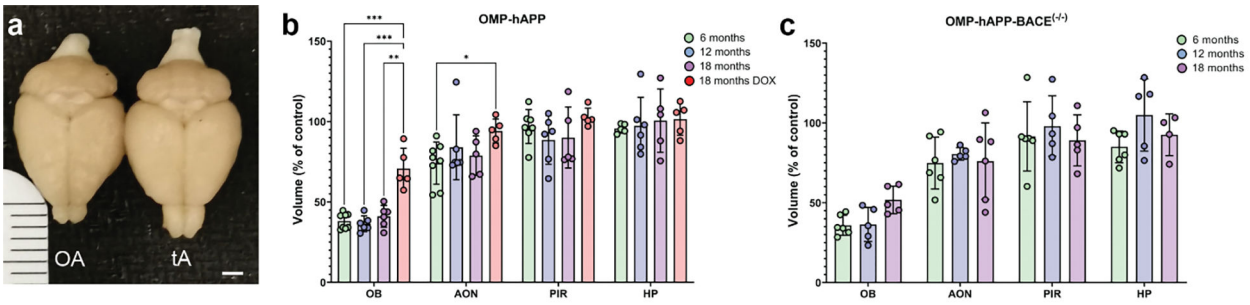

Figure 4. Volume analysis of olfactory regions of interest in OMP-hAPP and OMP-hAPP-BACE$^{(-/-)}$ mice.

(a) Representative brains from an OMP-hAPP and teto-hAPP mouse at 12-months old demonstrating the difference in gross OB structure and size. (b-c) Interleaved scatter with bars plot of volume expressed as percent average volume of control animals for OMP-hAPP (b) and OMP-hAPP-BACE$^{(-/-)}$ (c) animals at each time point. Points represent individual animals, bars represent mean ± SD. Two-way ANOVA was used with Tukey's multiple comparisons test to compare the means of each timepoint for each ROI. See Supplementary Table S3 for data on volume for each ROI and animal group. Abbreviations: OA, OMP-hAPP; tA, teto-hAPP; olfactory bulb, OB; anterior olfactory nucleus, AON; piriform cortex, PIR; hippocampus, HP. Scale bar (a) 2mm. *P ≤ 0.05, **P ≤ 0.01, ***P ≤ 0.001, ****P ≤ 0.0001.

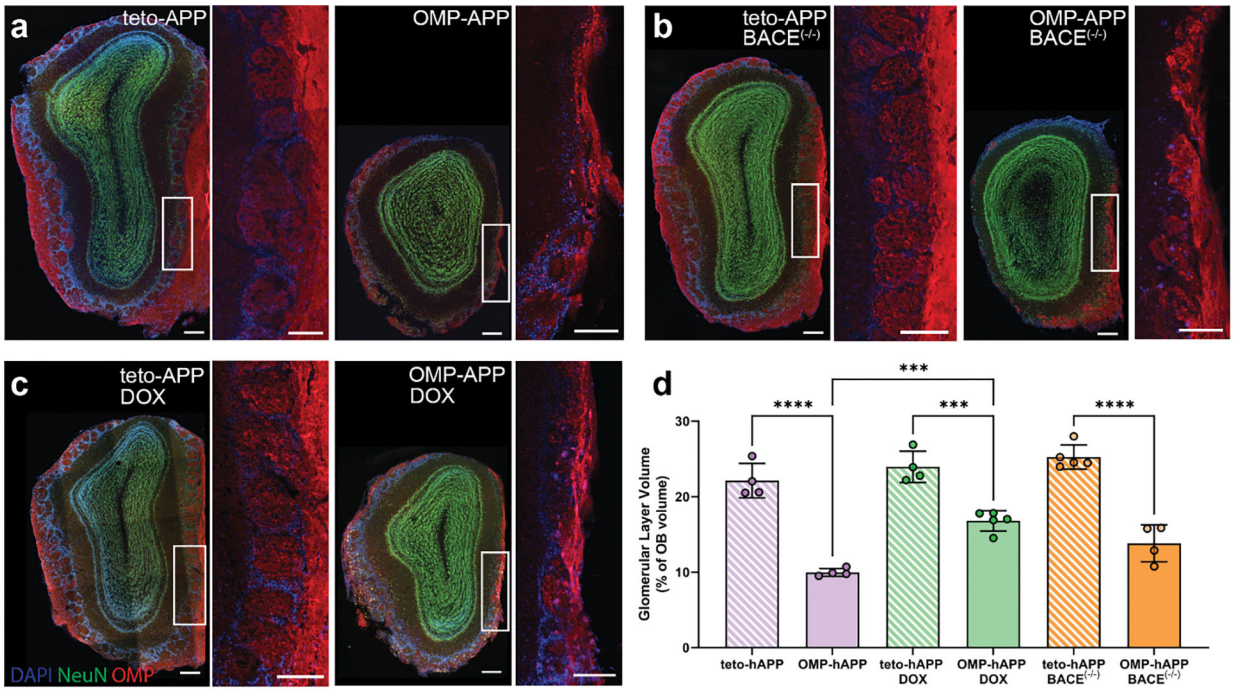

Figure 5. Glomerular layer volume in 18-month-old OMP-hAPP mice.

(a-c) Representative images of coronal OB sections from 18-month OMP-hAPP (a), OMP-hAPP-BACE$^{(-/-)}$ (b) and OMP-hAPP Dox pre-treated animals (c) and their respective teto-hAPP controls, labelled for DAPI (blue), NeuN (green) and OMP (red). The glomerular layer (inset) is thin and disorganized in all OMP-hAPP groups compared to controls. (d) Interleaved scatter with bars plot of the glomerular layer volume as a percentage of total bulb volume for 18-month-old OMP-hAPP and OMP-hAPP Dox pre-treated mice and their respective controls. Points represent individual animals, bars represent mean ± SD. Scale bars (a-c) 200 μm, (a-c inset images) 100 μm.

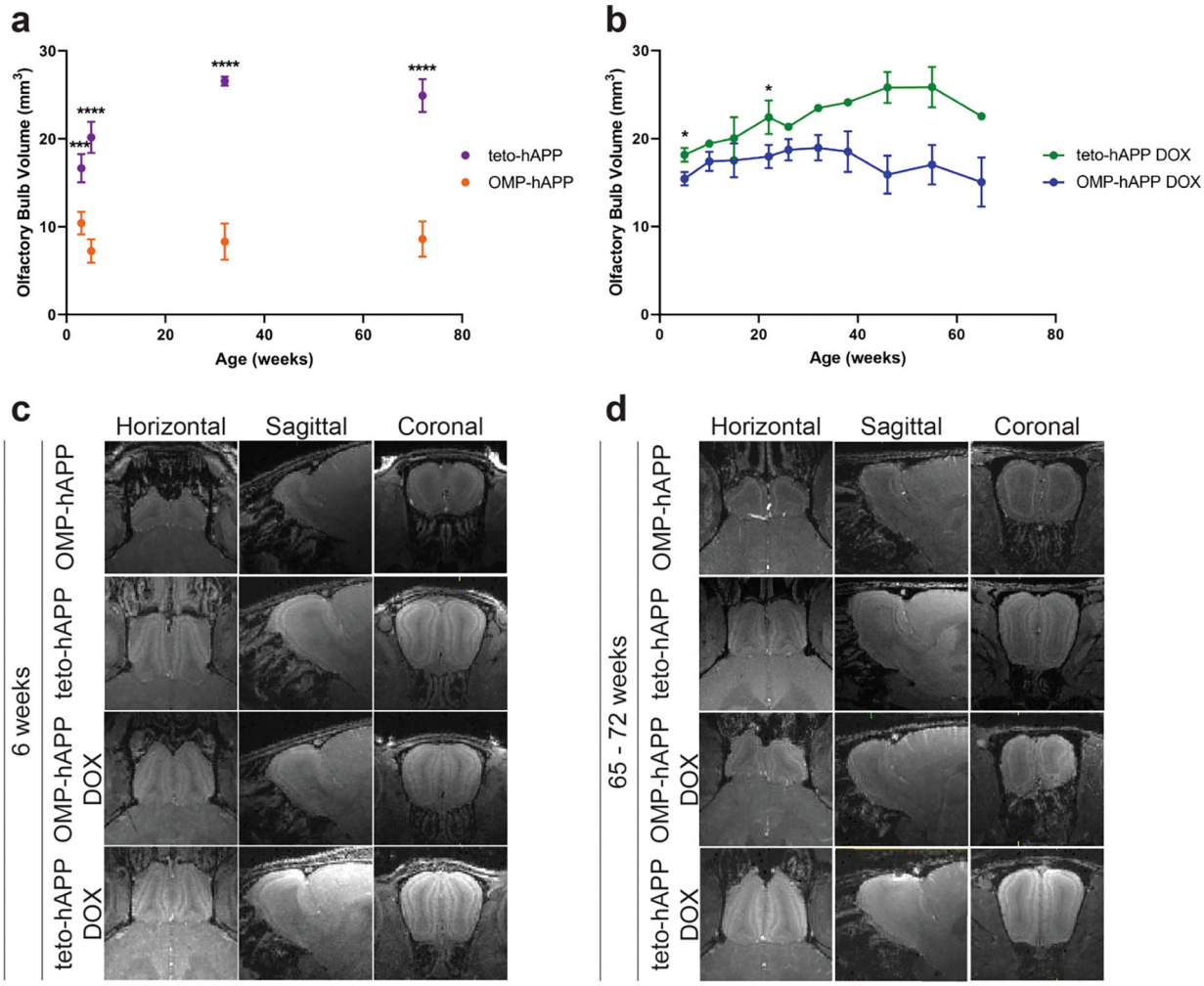

Figure 6. Olfactory bulb volume analysis from MEMRI of OMP-hAPP mice.

(a) Total olfactory bulb volume for teto-hAPP and OMP-hAPP mice at 3, 6, 32 and 72 weeks old. Different groups of mice were studied for each time point so points are not connected. (b) Time course of total olfactory bulb volume for teto-hAPP and OMP-hAPP mice that were treated with Dox until 3 weeks of age to prevent hAPP expression until weaning. The same mice were scanned at regular 6–8 week intervals from 6 weeks to 65 weeks. Values plotted represent mean ± SD for each group at each time point. (c-d) Representative horizontal, sagittal and coronal T1 weighted images (MEMRI), at 50 μm isotropic resolution, acquired 24 hours after i.v. infusion of 100mM $MnCl_2$ at 6 weeks old (c) and 65 weeks old (Dox pre-treated group) or 72 weeks old (OMP-hAPP group). **P ≤ 0.01, ***P ≤ 0.001, ****P ≤ 0.0001.

Table 1:

Details for the primers used in this study

Accession Number	Gene		Sequence (5'–3')	Amplicon Length
NM_000484.4	*APP* (human)	Fw	CCCGCTGGTACTTTGATGTGA	157
		Rv	AGAGGTTCCTGGGTAGTCTTGAGT	
NM_001198823.1	*APP* (mouse)	Fw	TGTGCCAGCCAATACCGAAA	86
		Rv	CAGAACCTGGTCGAGTGGTC	
NM_001289726.1	*GAPDH* (mouse)	Fw	TGTGTCCGTCGTGGATCTGA	77
		Rv	CCTGCTTCACCACCTTCTTGA	